ELSEVIER

Chemical Engineering Journal 135S (2008) S219–S228

Chemical Engineering Journal

www.elsevier.com/locate/cej

Numerical and experimental investigations of liquid mixing in T-type micromixers

A. Soleymani *, E. Kolehmainen, I. Turunen

Department of Chemical Technology, Lappeenranta University of Technology, P.O. Box 20, FIN-53851 Lappeenranta, Finland

Abstract

Three-dimensional numerical simulation was performed to study the flow dynamics and mixing characteristics of liquids inside T-type micromixers. The effects of various operating and design parameters on the flow dynamics and the quality of mixing were investigated qualitatively in order to optimize the mixing. Simulation results indicated that the development of vortices is essential to achieve good mixing performance. Furthermore, it was shown that the development and occurrence of vortices strongly depends on the flow rate and the geometrical parameters of the mixer, such as the aspect ratio, mixing angle and throttle size.

Experiments showed that the quality of mixing in the new mixers was significantly better than in ordinary T-mixers.

Keywords: Computational fluid dynamics; Micromixers; T-mixer; Mixing efficiency; Numerical diffusion

1. Introduction

The performance of most microchemical devices strongly depends on the efficiency of mixing, especially when dealing with fast reactions. Optimization of the mixing part is therefore needed to enhance the efficiency of a micro process [1–3]. In microscale, the mixing of the gas phase is entirely ensured by the molecular diffusion mechanism at low Reynolds number regimes. However, when dealing with a liquid phase, fast mixing remains a challenge owing to the small diffusion constants of the liquids [4].

Over the past decade, computational methods have proven to be an effective tool in the design and development of microprocesses. When simulating mixing processes with computational fluid dynamics, the convection-diffusion equations have to be solved numerically. An unphysical phenomenon, the so-called numerical diffusion, then often appears [5] which limits the accuracy of the results. A dimensionless group determining the strength of numerical diffusion is the cell-based Peclet number to which the dimension of a grid cell enters as the length scale. When considering mass transfer in gases, the cell size can often be chosen small enough to suppress numerical diffusion artifacts. However, computation of liquid mixing is not as straightforward, especially with moderate Reynolds numbers and with dimensions of hundreds of micrometers. In such cases, the resulting mesh will induce computational limitations due to the molecular diffusion constant, which is about four orders of magnitude smaller than in the gas phase. In this regard most of the simulation work on micromixers reported in the literature are devoted to gases phases with characteristic diffusion coefficients in the order of 10^{-5} m^2 s^{-1} [6].

Three-dimensional numerical simulation was performed to study flow dynamics and mixing characteristics of the liquid phase inside T-type micromixers. As shown in Fig. 1, a T is formed by two opposing liquid streams entering against each other and leaving through a channel that is perpendicular to the entry direction. Although the T-shaped micromixer geometry is simple, the hydrodynamics and the corresponding mass transfer is a three-dimensional problem [7] and a detailed look onto the underlying phenomena is still missing [8].

Bökenkamp et al. [9] and Engler et al. [1] performed sets of experiments in a T-shaped configuration and concluded that complete mixing is only achieved in the high Reynolds number regime with convection as the main mixing mechanism. In light of this finding, the major parts of the simulation were carried out at moderate and high Reynolds number regimes. The objective was to optimize the performance of the T-mixers for liquid phase applications. The effects of various operating and design parameters, such as volume flow rate, aspect ratio of the mixing channel or the mixing angle on the flow dynamics and the mixing efficiency were studied. In order to minimize the numerical diffusion, several ideas were applied. By utilizing the

* Corresponding author. Tel.: +358 5 62111; fax: +358 5 621 2199.
E-mail address: azita@lut.fi (A. Soleymani).

1385-8947/$ – see front matter © 2007 Elsevier B.V. All rights reserved.
doi:10.1016/j.cej.2007.07.048

Nomenclature

a	throttle size
C_i	concentration for ith cell in the cross sectional of interest
$\bar{C}$	equilibrium concentration
d_h	hydraulic diameter
D	molecular diffusion coefficient
Eu	Euler number defined as $\Delta P/\rho U^2$
H	height of mixing channel
ΔH_i	heat of the reaction
k_i	kinetic constants
K	identification number
l	characteristic length
L_C	extension of a computational cell
n	number of grid points in the cross sectional of interest
$\mathbf{n}$	unit vector outer normal to the side wall
P	pressure
Re	Reynolds number $\rho U d_h/\mu$
t	time
U	local flow velocity
$\mathbf{V}$	velocity vector
W_{out}	width of mixing channel

Greek letters

α	the mixing efficiency
μ	viscosity
ρ	density
$\boldsymbol{\tau}$	shear stress
σ^2	variance of concentration
σ^2_{max}	maximum variance of the mixture

results obtained from numerical calculations, a new family of T-mixers was then designed. A series of micromixers were fabricated to create a suitable experimental setup for validation of the simulation results.

2. Simulation method

The model used considers laminar mixing of the species in a T-type micromixer resulting from the contact between two identical fluids having the same viscosity, μ and the same density, ρ. The changes in mass, momentum, and concentrations of each species are described by

$$\nabla \cdot \mathbf{V} = 0, \tag{1}$$

$$\rho \frac{D}{Dt}\mathbf{V} = -\nabla P - \nabla \cdot \boldsymbol{\tau}, \tag{2}$$

$$\frac{D}{Dt}C_i = \nabla \cdot (D \cdot \nabla C_i) \tag{3}$$

where $\mathbf{V}$, D, and C_i are the velocity vector, molecular diffusion coefficients of the species and temporally and spatially varying concentration of species i, respectively. The fields of velocity and concentrations in the three-dimensional T-mixers as schematically illustrated in Fig. 1 were sought through discretization of the conservation equations (1)–(3) using the finite volume formulation [10]. A uniform velocity profile was assumed at the inlets and the pressure at the exit was assumed to be fixed to the local atmospheric pressure. No-slip boundary condition at the side walls was applied and the boundary condition on the concentrations at the side walls was simply $\partial C_i/\partial \mathbf{n} = 0$ which follows from the assumption that the wall boundary prohibits the species undergoing diffusion. Here, $\mathbf{n}$ is the unit vector outer normal to the side wall. The concentration of species 1, C_1 was imposed as 0 at one inlet and as 1 at the other. The Simple-Consistent algorithm [11] was implemented for pressure–velocity coupling. In order to reduce discretization artefacts, all the spatial discretizations were performed using the QUICK scheme [12] in conjunction with a second-order implicit-in-time discrete differentiation.

The computations were done in two stages. First, the continuity and momentum equations were solved numerically to obtain the velocity profile that was eventually inserted into the convection-diffusion equation. Then the solution of the latter provided the concentration distribution inside the whole domain. In this set of simulations, both liquids entering into the T-mixers had identical physical properties ($\rho = 998.2\,\mathrm{kg\,m^{-3}}$, and $\mu = 0.001\,\mathrm{Pa\,S}$).

In order to quantify the extent of the mixing at a certain cross-section of the mixing channel, the ratio of variance of concentration, σ^2 and the maximum variance of the mixture, σ^2_{max} can be considered. The mixing efficiency is then defined by

$$\alpha = 1 - \sqrt{\frac{\sigma^2}{\sigma^2_{max}}} \text{ with } \sigma^2 = \frac{1}{n}\sum_{i=1}^{n}(C_i - \bar{C})^2, \tag{4}$$

where $\bar{C}$ is the mean value of the concentration field, C_i is the concentration for ith cell in the cross sectional area of interest, and n is the number of grid points inside the cross-section. A value of 1 for α indicates perfect mixing, whereas $\alpha = 0$ means that no mixing has occurred. In this paper all the values for the mixing efficiency α were calculated for the outlet of the mixers.

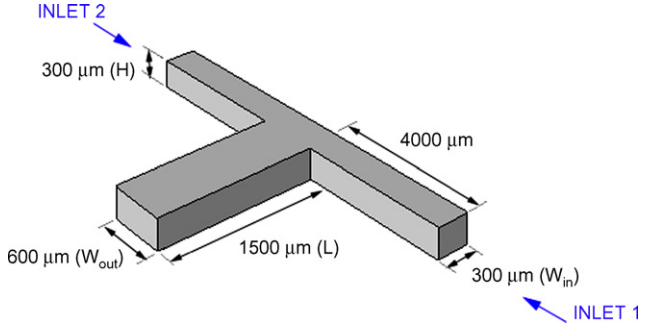

Fig. 1. Schematic picture of the T-mixer.

Table 1
Effect of the mesh Peclet number on the mixing efficiency calculations for maximum Reynolds number of the present study

Re	D ($m^2\ s^{-1}$)	U_{max} ($m\ s^{-1}$)	$Pe_{mesh,max}$	Mixing efficiency (%)	Variation (%)
240	2×10^{-7}	1.41	12	78.9	
			24	79.3	0.5
			48	84.2	5.8

2.1. Grid refinement

Discretization of the convective terms in the transport equation of concentration fields introduces numerical diffusion [5] which limits the accuracy of the numerical prediction. It is particularly important at high flow rates in liquid mixing with characteristic diffusion constants in the order of $10^{-9}\ m^2\ s^{-1}$, inducing cell Peclet numbers that are too high for convection-diffusion calculations. Here, the cell Peclet number is defined as UL_C/D, where U is the local flow velocity, L_C and D are cell size (extension of a computational cell) and diffusion coefficient, respectively. In the present study, in order to suppress artifacts from numerical diffusion, all the spatial discretizations were performed using a higher-order discretization scheme (QUICK) [10,12] and the mesh Peclet number was fixed at moderate values. In order to maintain a moderate Peclet number, the local mesh size needed to be quite small which in the channels of dimensions of hundreds of micrometers results in a large number of grid points. Therefore, performing three-dimensional simulations with very small cell size does not seem to be feasible due to the computational intensity that would be involved. As a remedy, following [3], the diffusion constant was artificially increased. Moreover, the mesh was locally refined. Initially the simulations were performed with body-fitted structured grids of length 8 μm in all directions. The grids were then locally refined in the area where the cell Peclet number was high. A Peclet number of 24 was used as the basis for mesh refinement. The non-influence of the mesh Peclet number on the results was verified for different calculations and its results for the highest value of Reynolds number, whose numerical error was maximum, are presented in Table 1.

The mixing performance was different for $D = 10^{-9}\ m^2\ s^{-1}$ (typical liquid diffusion constant) and those diffusion coefficients used in the simulations, and therefore the simulation results are not quantitatively correct. However, they describe the trends of the phenomena and were used only in the optimization of the mixers. The quantitative values for the mixing performance were obtained from experiments.

3. Simulation results

3.1. Base case

Detailed dimensions of the base case are shown in Fig. 1. To achieve realistic simulations, the lengths of the side branches were chosen long enough not to influence significantly the simulation of the fluid behaviour inside the mixer channel. The velocities at both inlets were $0.4\ m\ s^{-1}$, corresponding to a Reynolds number of 120 based on the hydraulic diameter of the inlet channels. All other simulations were variations of this case.

3.2. Variation in volume flow rate

Simulations were performed to investigate the effects of volume flow rate on the flow dynamics and mixing in the mixer shown in Fig. 1. The inlet liquid velocities of both streams were equal and varied from 0.01 to $0.8\ m\ s^{-1}$. The mixing performance α is shown as a function of Reynolds number in Fig. 2. Here, the Reynolds number is defined based on the average velocity in the mixing channel and the hydraulic diameter of the mixing channel. As seen in Fig. 2 the trends are the same for both values of the diffusion constant and denoted are the three different laminar flow regimes.

At very low Reynolds numbers where the flow is strictly laminar (stratified flow), the mixing is entirely due to molecular diffusion between the layers of different concentrations (Fig. 3a and d). As the volume flow rate increases in the stratified regime, the residence time of the fluids decreases inducing the deduction of the mixing efficiency. For moderate Reynolds numbers an increase in the mixing efficiency sets in, indicating that the flow patterns change and convective mass transfer promotes mixing. However, the main mixing principle is still diffusion and the symmetry plane perpendicular to the inlet channels is preserved (Fig. 3b and e). At higher values of Reynolds number, complex convection-dominated mixing mechanisms are observed and the

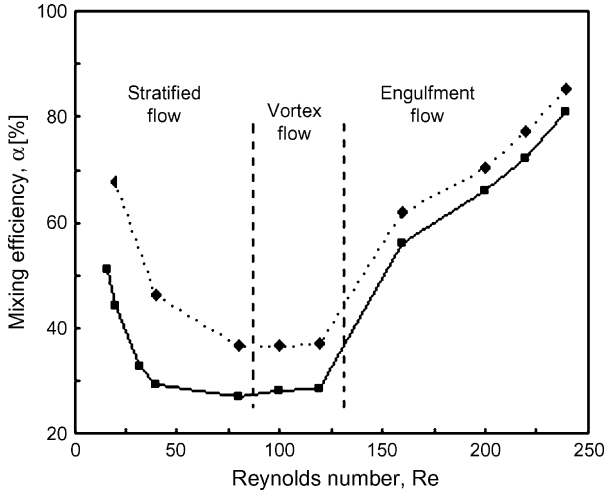

Fig. 2. Variation of mixing quality α as a function of Reynolds number. Squares and diamonds represent the numerical results with $D = 2 \times 10^{-7}\ m^2\ s^{-1}$ and $D = 1 \times 10^{-6}\ m^2\ s^{-1}$, respectively.

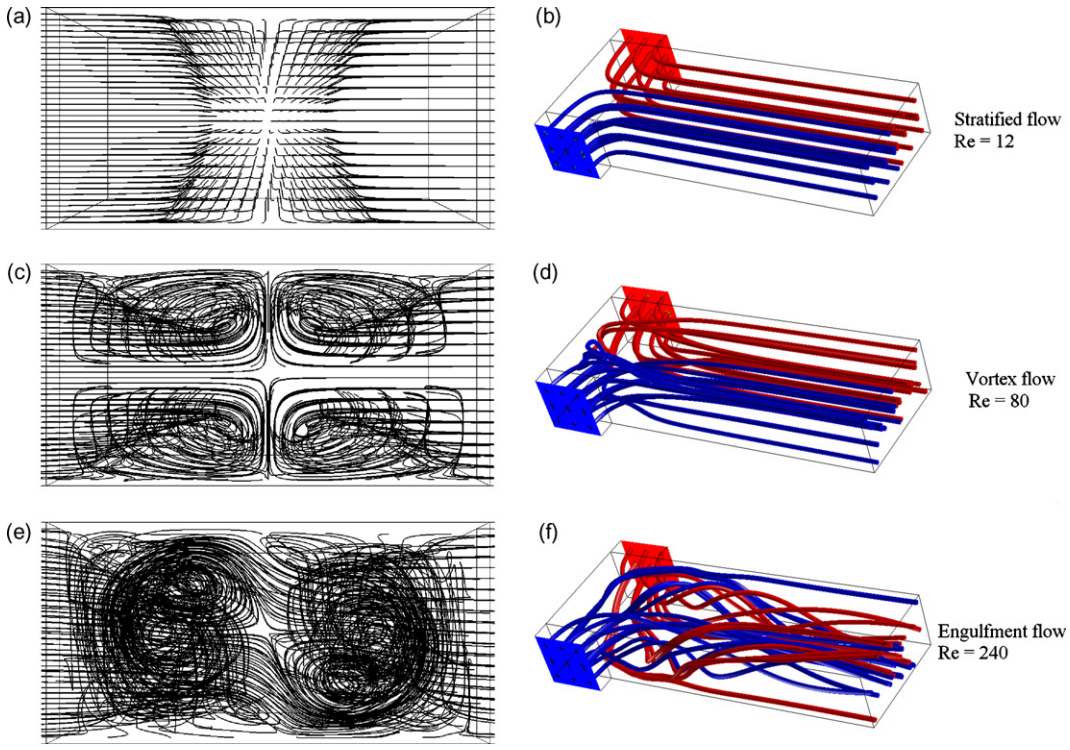

Fig. 3. Path lines at the entrance of the mixing channel for different flow regimes namely, stratified, vortex and engulfment flow. (a), (b) and (c) correspond to $Re = 12$, $Re = 80$ and $Re = 240$, respectively. Although the different flows are all in the laminar range there is a development of vortices with increasing Reynolds numbers. A better understanding of the flow field, can be deduced from the streamlines presented in (d)–(f). Colour is used to distinguish between the streams entering each of the inlet channels. As shown in (f) the swirling of the fluid flow results in dragging fluids from the middle to the top and bottom sides of the mixer. This engulfment of the streamlines leads to a very high improvement in the mixing quality.

axial symmetry breaks up (Fig. 3c and f). The generated vorticity increases the contact area of the components and reduces the mixing distance. Since diffusion over small distances is fast, rapid mixing is achieved.

For the three different flow regimes, namely stratified, vortex and engulfment regimes, the variation in the cross-sectional pressure along the mixing channel length is shown in Fig. 4. As seen in Fig. 4a, the flow in the stratified regime is roughly of linear pressure dependence along the axial direction. This behaviour is similar to the laminar flow in straight ducts and it can be attributed to the fact that the flow is strictly laminar.

For a moderate Reynolds number where the flow is in the vortex regime, the values of the pressure are sharply decreased at the mixing zone due to deflection of the inflowing streams (Fig. 4b). After the mixing zone, however, a linear pressure dependence is observed as expected for fully developed duct flow (Fig. 3e). This varying dependence in the pressure drop along the mixing channel allows for determination of the mixing zone defined as the region where convection (formation of vortices) is the main mixing process.

As depicted in Fig. 4c, by increasing the Reynolds number the mixing zone becomes larger and the pressure drop significantly increases. As a result of the high pressure drop observed in the mixing zone, a relatively large energy input is needed for the deflection of the flow into the mixing channel and to build up the vortex structure.

3.3. Mixing angle variation

Numerical simulations of liquid mixing in a T-mixer with a number of mixing angles ranging from 30 to 135° were carried out. All parameters were kept the same except the mixing angle, defined as half of the angle at which the two inlet channels meet. Results for different mixing angles are shown in Table 2.

Again the same trends were observed for different diffusion constants. The results show that the pressure drop along the mixing channel increased with the mixing angle. Furthermore, changing the angle of mixing had a significant effect on the mixing. The mixing efficiency was increased when an angle of 90 or 105° was used. This can be attributed to the fact that for the engulfment flow regime, there is an optimum T-angle around 90 or 105° for which the strength of the vorticity reaches a maximum (see Fig. 5).

This finding is in contrast to the mixing of gas phase, for which the mixing angle has no significant effect on the mixing [6]. One explanation is that the mixing of the gas phase in the range of Reynolds numbers studied in [6] is ensured by molecular diffusion.

3.4. Variation in aspect ratio

Simulations were performed to investigate the effects of the aspect ratio of the mixing channel, defined as H/W_{out}, on the

Table 2
Simulation results for different mixing angles

Mixing angle	Mixing efficiency, α ($D = 2 \times 10^{-7}$ m^2 s^{-1})	Mixing efficiency, α ($D = 1 \times 10^{-6}$ m^2 s^{-1})	Pressure drop (Pa)
30	16.2	21.9	275
45	16.4	22.2	305
60	23.5	30.9	335
75	26.0	34.0	371
90	56.0	61.9	410
105	60.3	88.4	461
120	33.3	40.4	482
135	31.2	37.7	520

flow patterns and mixing efficiency in the T-type micromixers described in Fig. 1. For all the simulations in this section, the channel width W_{out} was kept constant at 600 μm and the inlets velocities at 0.4 m s^{-1}. For the studied aspect ratio range the pressure drop along the mixing channel was varied from 293 to 26866 Pa. The mixing efficiency α is shown as a function of the aspect ratio in Fig. 6. The results indicate that there is an optimum aspect ratio at which α reaches a maximum value. This can be explained by the change in the flow patterns and the development and appearance of the vortices (Fig. 7). At very low aspect ratio (Fig. 7a and e), the flow inside the mixing channel flows in the stratified regime due to the high wall friction of the fluid, which results in high values of pressure drop. As molecular diffusion is the only mixing mechanism, the mixing quality is very low.

By increasing the aspect ratio, the pressure drop decreases and changes in the flow patterns are observed namely, a transition from stratified flow to vortex flow (Fig. 7b and f) and then to engulfment flow (Fig. 7c and g). At the optimum aspect ratio, the formation of the vortices reaches a maximum value which results in a maximum value for the mixing efficiency. After the optimum point, increasing the aspect ratio leads to damping of the vortices (Fig. 7d and h) and therefore decreasing mixing efficiency.

From the dependency of the mixing efficiency (or flow patterns) on the aspect ratio, it can be concluded that the development and appearance of vortices depends not only on the Reynolds number, which increases with aspect ratio, but also on another dimensionless group accounting for the pressure loss (origins from the vortex creation and the wall friction of the fluids).

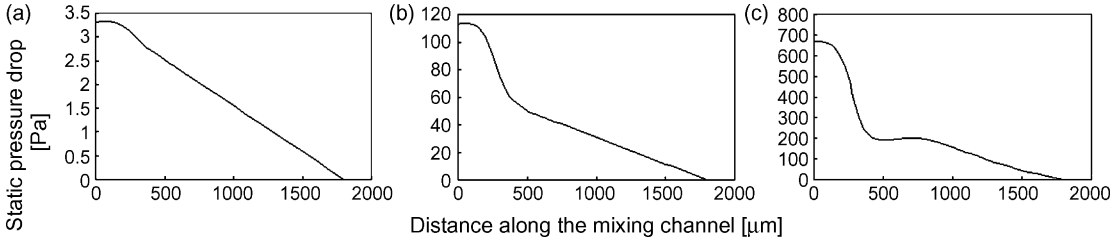

Fig. 4. Cross-sectional pressure average over the mixing channel for (a) $Re = 12$; (b) $Re = 80$; and (c) $Re = 240$.

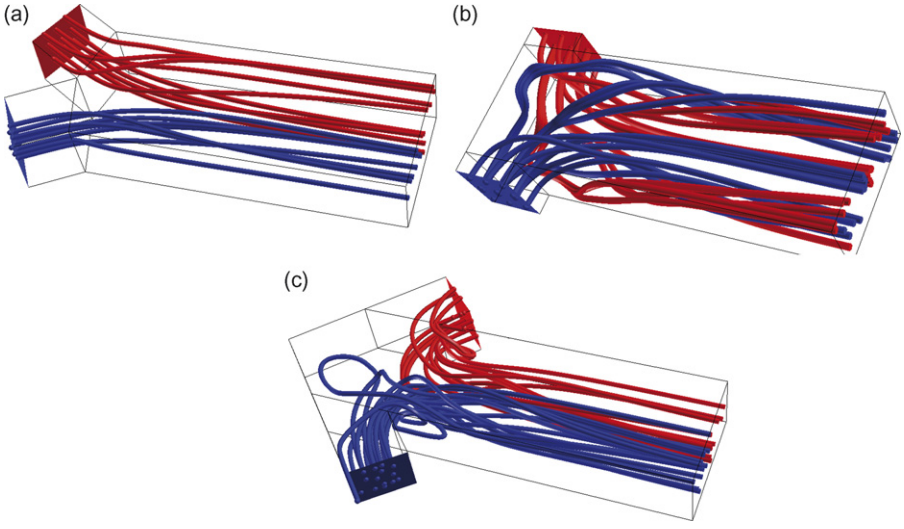

Fig. 5. The streamline patterns inside of the mixing channel for mixing angles (a) $\theta = 30°$; (b) $\theta = 90°$; and (c) $\theta = 135°$. Colour is used to distinguish between the streams entering the mixing channel from each inlet channel.

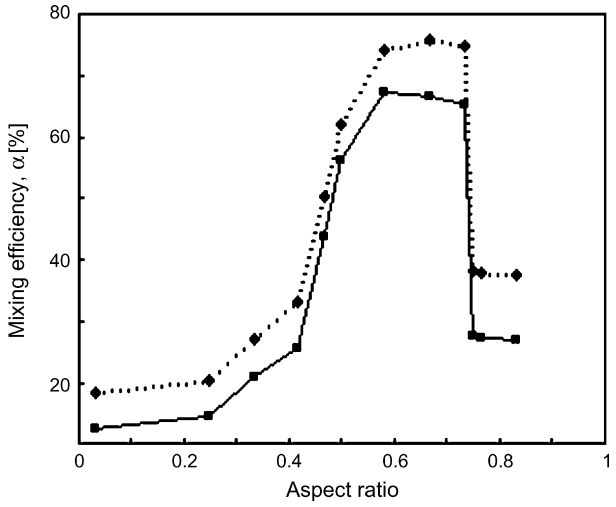

Fig. 6. Mixing efficiency α as a function of aspect ratio. Squares and diamonds represent the numerical results with $D = 2 \times 10^{-7}\,m^2\,s^{-1}$ and $D = 1 \times 10^{-6}\,m^2\,s^{-1}$, respectively. As depicted the trend for both diffusion constants are the same.

The present results could be more precise if a change in W_{out} could be taken into account. Such considerations will be discussed in a future paper.

3.5. Throttle T-mixer

A schematic diagram of the throttle mixer can be seen in Fig. 8. The throttle size was varied from 150 to 600 μm, while the inlet liquid velocities were kept constant at $0.4\,m\,s^{-1}$.

Variation in mixing efficiency α as a function of the throttle size is shown in Fig. 9. The curve indicates the minimum point at about 400 μm which can be attributed to the changes in the flow patterns and the residence time of the flow inside the mixing channel.

At $a = 600$ μm (Fig. 10a) for which the mixing channel is perpendicular to the inlet channels, the flow inside the mixing channel flows in the engulfment regime (asymmetric path lines). As stated earlier, the engulfment of the streamlines leads to a very high improvement in the mixing quality.

By decreasing the throttle size from 600 to 400 μm, the simulations show that vortices are more dampened with a lower throttle (Fig. 10a–c). This results in a decrease in the mixing efficiency.

As shown in Fig. 10c at $a = 400$ μm, the flow is in the vortex regime in which path lines have axial symmetry to the mixing channel. Below the minimum point, mixing becomes more efficient with decrease in throttle size. This can be attributed to the decrease in the diffusional distance [13] and the change in flow pattern to engulfment flow (Fig. 10d). A decrease in the throttle size in this range introduces a relatively large pressure drop. Thus a trade-off between the throttle size and the pressure drop has to be made. The pressure drop along the mixing channel varied between 410 and 2245 Pa for the largest and smallest throttle size, respectively.

4. Experimental studies

4.1. Test reaction

There are several ways to determine the performance of different mixers. Here, a method called the fourth Bourne reaction system was employed. It is based on competition between the following two parallel reactions:

$$HCl + NaOH \xrightarrow{k_1} NaCl + H_2O \quad (5)$$

$$H_3CC(OCH_3)_2CH_3 + H_2O \xrightarrow{k_2/H^+} (CH_3)_2CO + 2CH_3OH \quad (6)$$

where $H_3CC(OCH_3)_2CH_3$ is 2,2-dimethoxypropane and $(CH_3)_2CO$ is acetone. Acid catalyzed hydrolysis of 2,2-dimethoxypropane (DMP) is carried out simultaneously with a neutralization reaction between HCl and NaOH. The result of these reactions depends not only on the reaction kinetics but also upon the speed of the mixing process. Consequently, the efficiency of mixers can be characterized by the yield of the reaction products. The lower the conversion of the latter reaction (6), the better is the mixing efficiency. At a temperature of 298 K the reactions are first-order with respect to each component and the kinetic constants are $k_1 = 1.4 \times 10^8\,m^3\,mol^{-1}\,s^{-1}$ and $k_2 = 0.584\,m^3\,mol^{-1}\,s^{-1}$ for reactions (5) and (6), respectively.

The heat of reaction (5) is $-55.8\,kJ\,mol^{-1}$. Reaction (6) is slightly endothermic having a reaction heat of $18.0\,kJ\,mol^{-1}$. Both reactions are irreversible. Detailed information for this reaction system has been given by Baldyga et al. [14].

4.2. Micromixer types

Two micro T-mixers with the same hydraulic diameters were studied. Their detailed dimensions are presented in Fig. 11. A third micromixer, termed TT-mixer, was developed and constructed utilizing the results of the numerical simulations (Fig. 12).

As seen from numerical results, the development of vortices is essential to good mixing in T-type micromixers. The formation of vortices in the mixing zone, defined as the region in which the convection is the main mixing process, arises through the influence of centrifugal forces. After the mixing zone, the flow is almost fully developed and the mixing merely occurs by a molecular diffusion mechanism. Consequently, in T-type micromixers mixing zones are the most effective parts of the mixers. In this regard, two junctions are adjusted in the proposed micromixer to enlarge the effective parts of the mixer and to increase the vortex generation. As depicted in Fig. 12 both feed streams have two inlet channels into the mixer, located opposite to each other. This splitting of the fluid flow also enlarges the contact surface area.

Applying the results of the numerical simulations, the mixing angles were set to 90° for both junctions. Moreover circular elements were adjusted in the mixing channel to enhance the vorticity, which resulted in better mixing.

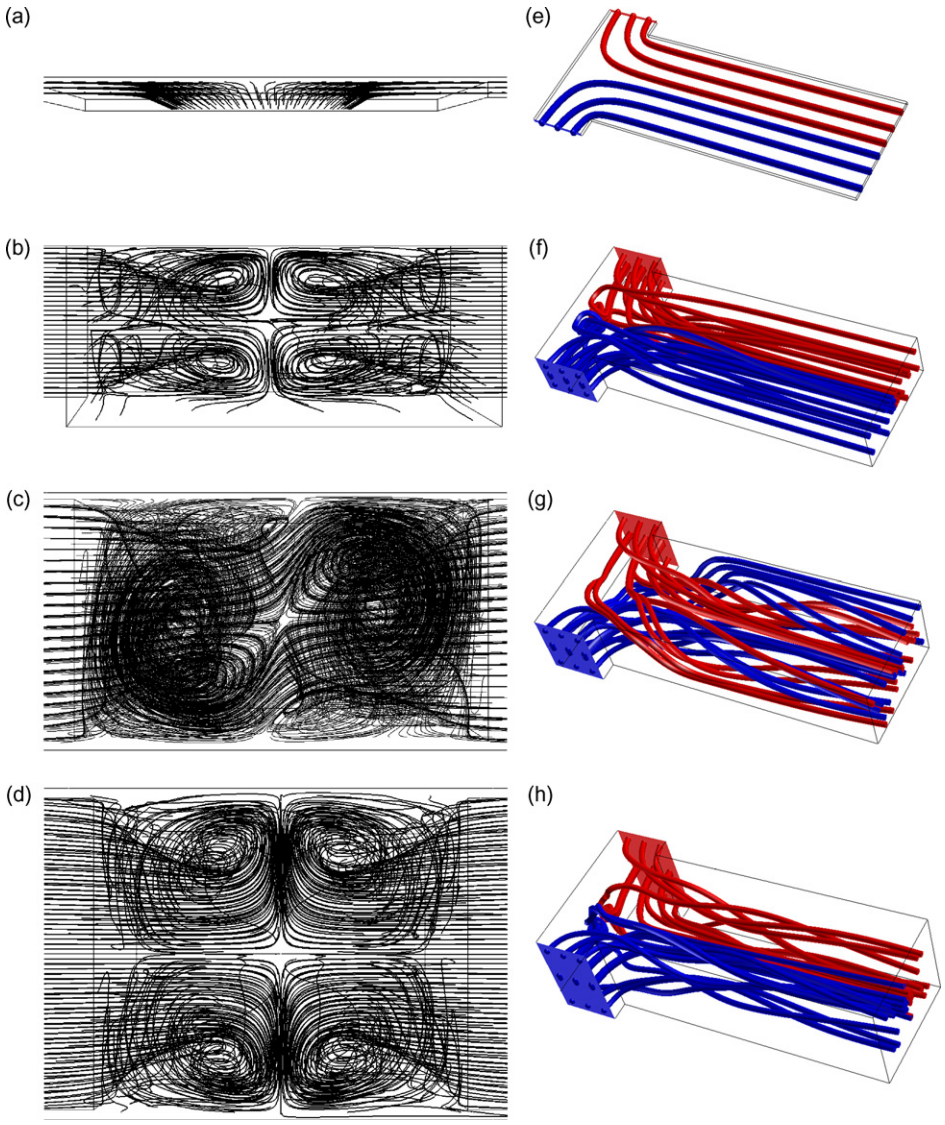

Fig. 7. Path lines at the entrance of the mixing channel for aspect ratio (a) 0.03; (b) 0.42; (c) 0.58; and (d) 0.83. The streamlines are presented in (e)–(h). Colour is used to distinguish between the streams entering the mixing channel from each inlet channel.

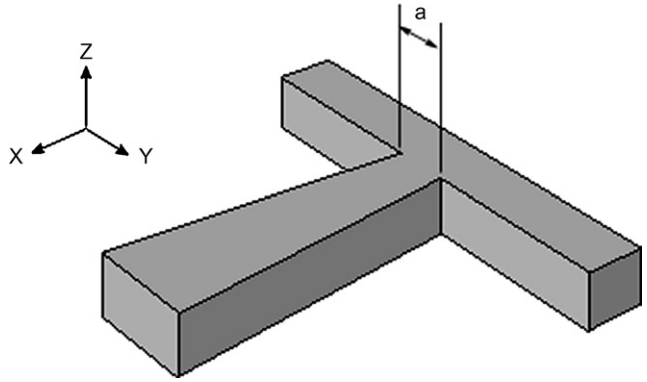

Fig. 8. Schematic picture of the throttle mixer.

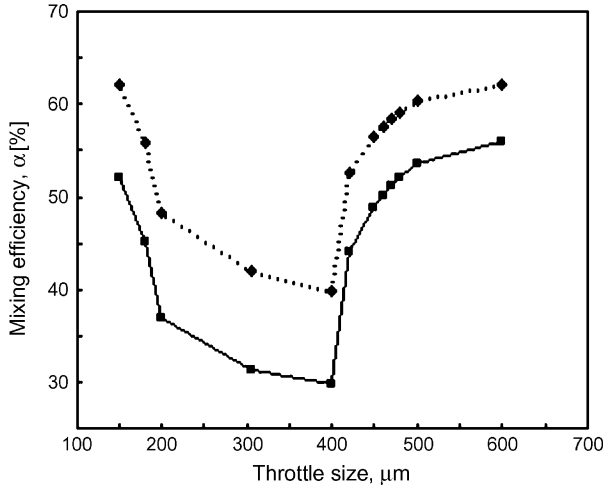

Fig. 9. Mixing efficiency as a function of the throttle size. Squares and diamonds represent the numerical results with $D = 2 \times 10^{-7}\ \mathrm{m^2\ s^{-1}}$ and $D = 1 \times 10^{-6}\ \mathrm{m^2\ s^{-1}}$, respectively.

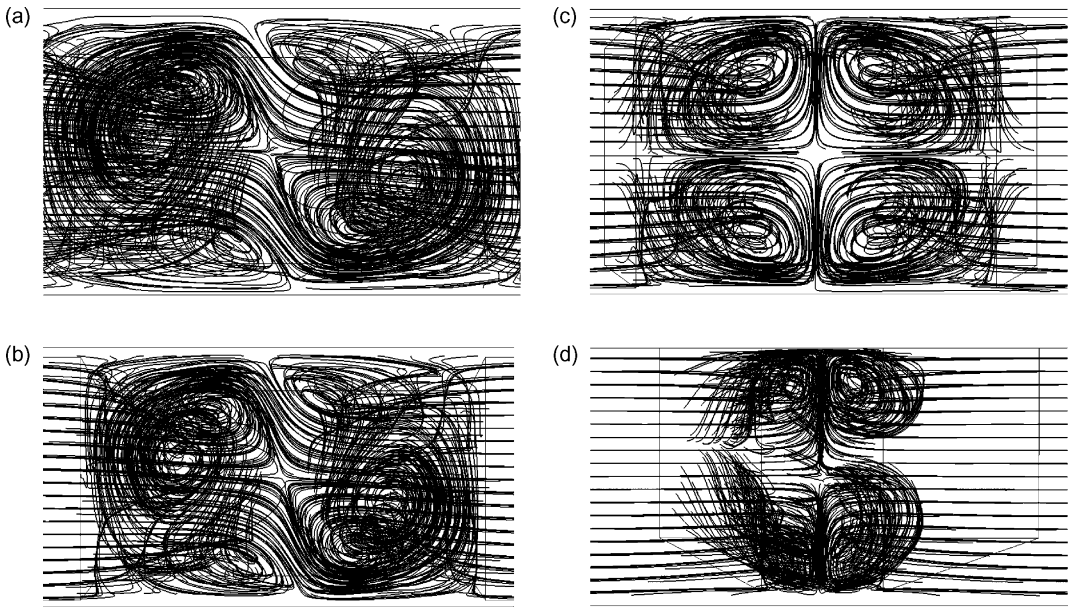

Fig. 10. Path lines at the entrance of the mixing channel for (a) $a = 150$; (b) $a = 400$; (c) $a = 500$; and (d) $a = 600$.

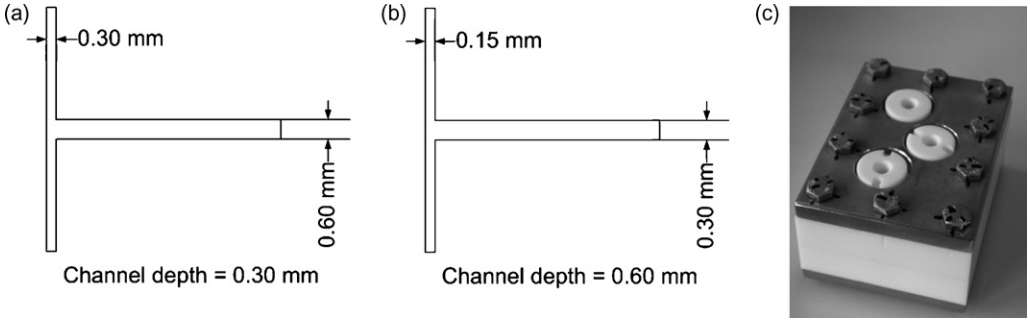

Fig. 11. Geometric data of the micro T-mixers used in the experimental study; (a) T-mixer (1); (b) T-mixer (2); (c) housing of T-mixers. Both mixers have the same hydraulic diameters.

The dimensions of the constructed TT-mixer are shown in Fig. 13. The channel depth of the TT-mixer and the diameter of the circular elements are 300 and 200 μm, respectively. Micromixers were manufactured by micromachining using PTFE (PolyTetraFluoroEthylene) as the main construction material. The mixers were fabricated by *high speed milling* (HSM).

In order to evaluate the efficiency of the proposed micromixer (TT-mixer), a set of experiments was carried out with a commercial multilamination micromixer, called SSIMM (Slit Interdigital MicroMixer SIMM-V2-HC22, produced by IMM GmbH). The results were then compared with those of the micro TT-mixer.

4.3. Experimental set-up

A schematic drawing of the experimental set-up is presented in Fig. 14. Pumps were connected to the mixer by 1.0 mm inner diameter PTFE tubing. Similar PTFE tubing was also connected to the outlet of the mixer. The mixer and outlet tube were immersed in a thermostatic bath, where the temperature was maintained at 298 K. In all the experiments, the total flow rate was in the range between 0.088 and 17.77 ml min^{-1}. This range corresponds to Reynolds numbers between 2 and 308 in the mixing chamber.

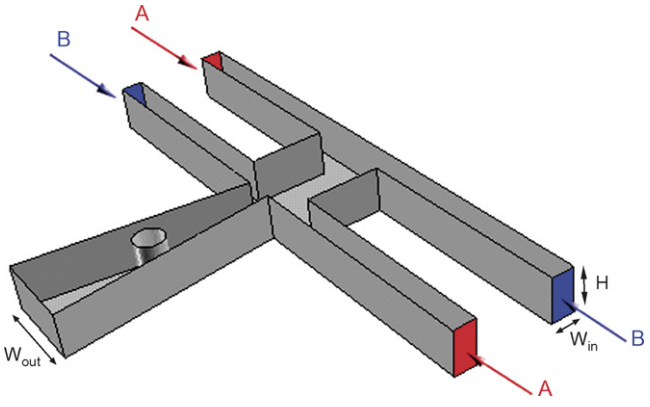

Fig. 12. Schematic picture of the optimized T-mixer, termed TT-mixer.

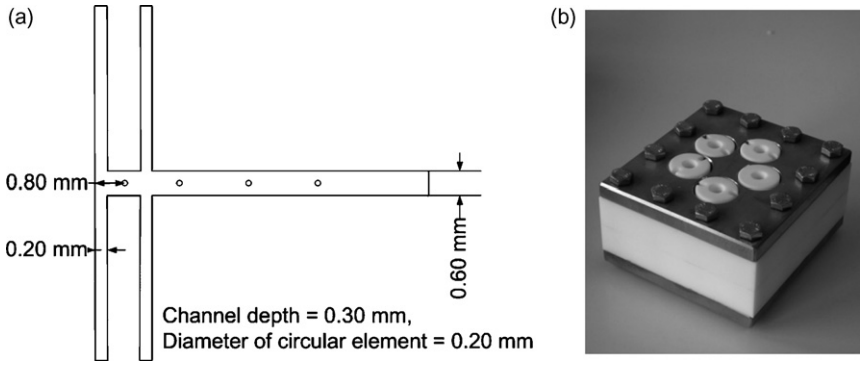

Fig. 13. The TT-mixer (a) the main dimensions; and (b) housing.

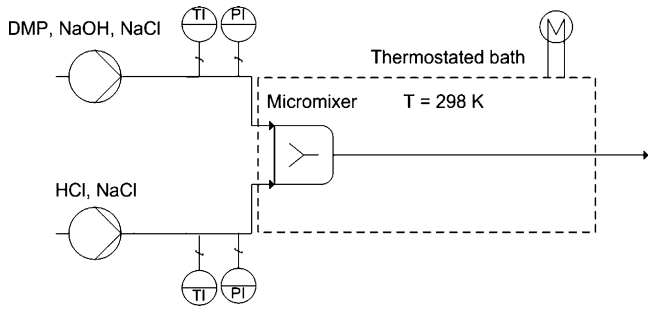

Fig. 14. Schematic drawing of the experimental set-up.

4.4. Experimental procedure

As shown in Fig. 14, two feed streams were used. One feed stream contained DMP, NaOH and NaCl and the other HCl and NaCl. 25 wt.% ethanol in de-ionized water was used as the solvent in both feed streams. The concentrations of the components in the feed streams were as follows: $C_{DMP} = 200\ mol\ m^{-3}$; $C_{NaOH} = 210\ mol\ m^{-3}$; $C_{HCl} = 200\ mol\ m^{-3}$ and $C_{NaCl} = 90\ mol\ m^{-3}$. All the experiments were carried out at 298 K.

The feed streams were pumped into the mixer and samples were taken from the outlet of the mixers. The samples were cooled down immediately and kept in ice until analysis. The reaction products were analyzed by means of a gas chromatograph (Agilent 6890N) with a flame ionization detector. The length of the column was 30 m and the inner diameter was 0.32 mm. Ethanol was used as an internal standard in the analysis.

5. Experimental results

Experimental results, representing the mixing efficiency of micromixers, are shown in Fig. 15. The lower the conversion of the second reaction (6), the better the mixing result.

From Fig. 15, three different mixing regimes can be distinguished. These might be interpreted as the stratified, vortex, and engulfment regimes observed in the numerical calculations. Moreover, the results clearly show that good mixing in all T-mixers is achieved at high flow rates. This finding is consistent with the observations in the simulations.

As depicted in Fig. 11 the hydrodynamic diameters of the mixing channel for both T-mixer (1) and T-mixer (2) are the same. Therefore, for a specific volume flow rate the Reynolds numbers in the mixing channels for both mixers are the same. In spite of the fact that T-mixer (1) has a mixing channel width twice wider than that of T-mixer (2), the experimental results show that for a specific Reynolds number the mixing quality in T-mixer (1) is much better than in T-mixer (2). This reveals that the geometric parameters, especially the aspect ratio of the mixer, have a significant effect on the development of vortices and therefore on the mixing efficiency. This experimental observation is con-

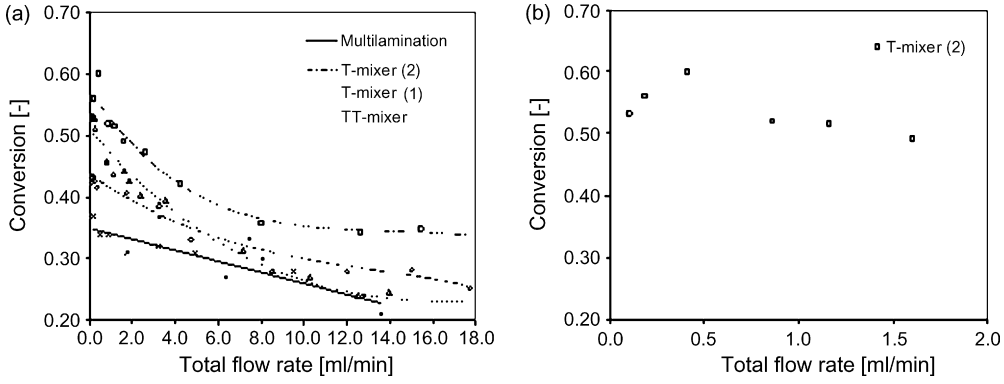

Fig. 15. Conversions as a function of volume flow rate for the tested mixers. To obtain better visualization of the stratified regime, the conversion for the T-mixer (2) at the low flow rates is magnified and represented in (b). The lower the conversion, the better the mixing result.

sistent with the numerical finding that the vortex generation and therefore mixing performance in T-type micro mixers depend not only on Reynolds number, but also on geometric parameters. In light of this in order to obtain effective mixing, careful consideration should be devoted to the design of T-mixers.

It can also be seen from Fig. 13 that at high flow rates the proposed T-mixer (TT-mixer) is much more effective than the ordinary T-mixers (1) and (2). Moreover, its mixing performance approaches that of the commercial micromixer (SSIMM) at flow rates higher than 8 ml min^{-1}.

6. Summary and conclusion

Flow dynamics and mixing characteristics of liquids in T-type micromixers were investigated. The aim was to develop a new effective T-type micromixer for the liquid phase. To optimize the mixer, the mixing behaviour was computed with various operating and design parameters by means of computational fluid dynamics. In order to suppress artifacts from numerical diffusion, the mesh Peclet number was fixed at moderate values by artificially increasing the diffusion constant and refining the mesh locally. This approach resulted in a qualitative study of the mixing performance. However, it did not affect the flow dynamics of the system and the development of vortices.

Simulation results proved that the development of vortices is essential for good mixing performance. Furthermore, it was shown that the development and occurrence of vortices depends strongly on both volume flow rates and geometrical parameters of the mixer such as the aspect ratio and mixing angle. This leads one to concluded that the appearance of the vortices depends not only on Reynolds number, but also on another dimensionless group accounting for pressure loss. In regards to this it merits to determine an identification number for the distinction of the different flow regimes and to find out the critical value for the identification number at which the transition from vortex flow (symmetric path lines) to engulfment flow (asymmetric path lines) occurs. These issues will be the subject of a future paper.

Utilizing the simulation results, a new simple and efficient micromixer was introduced (Fig. 12).

A set of experiments was carried out to support the simulation results. The mixing performance was characterized by the conversion of a secondary product in parallel competitive reactions. The numerical results were found to be consistent with experimental findings. The experimental results showed that the mixing efficiency obtained by the proposed mixer was much better than that of the ordinary T-mixers without an additional mixing element. The mixing efficiency of the proposed mixer was comparable to that of commercial, more complex and expensive micromixers.

References

[1] M. Engler, N. Kockmann, T. Kiefer, P. Woias, Numerical and experimental investigations on liquid mixing in static micromixers, Chem. Eng. J. 101 (2004) 315.
[2] St. Ehlers, K. Elgeti, T. Menzel, G. Wießmeier, Mixing in the offstream of a microchannel system, Chem. Eng. Process 39 (2000) 291.
[3] V. Mengeaud, J. Josserand, H.H. Girault, Mixing processes in a zigzag microchannel: finite element simulations and optical study, Anal. Chem. 74 (2002) 4279.
[4] J.B. Knight, Ashvin Vishwanath, J.P. Brody, R.H. Austin, Hydrodynamic focusing on silicon chip: mixing nanoliters in microseconds, Phys. Rev. Lett. 17 (1998) 3863.
[5] B. Noll, Numerische Strömungsmechanik, Springer, Berlin, 1993.
[6] D. Gobby, P. Angeli, A. Gavriilidis, Mixing characteristics of T-type microfluidic mixers, J. Micromech. Microeng. 11 (2001) 126.
[7] M. Hoffmann, M. Schluter, N. Räbiger, Experimental investigation of liquid–liquid mixing in T-shaped micro-mixers using μ-LIF and μ-PIV, Chem. Eng. Sci. 61 (2006) 2968.
[8] D. Bothe, C. Stemich, H. Warnecke, Fluid mixing in a T-shaped micromixer, Chem. Eng. Sci. 61 (2006) 2950.
[9] D. Bökenkamp, A. Desai, X. Yang, Y. Tai, E. Marzluff, S. Mayo, Microfabricated silicon mixers for submillisecond. Quench-flow analysis, Anal. Chem. 70 (1998) 232.
[10] S.V. Patankar, Numerical Heat Transfer and Fluid Flow, McGraw-Hill, New York, 1980.
[11] J.P. Vandoormaal, G.D. Raithby, Enhancements of the SIMPLE Method for Predicting Incompressible Fluid Flows, Numer. Heat Transfer 7 (1984) 147.
[12] B.P. Leonard, A stable and accurate convective modeling procedure based on quadratic upstream interpolation, Comp. Mech. Appl. Eng. 19 (1979) 59.
[13] T.T. Veenstra, T.S.J. Lammerink, M.C. Elwenspoek, A. Berg, Characterization method for a new diffusion mixer applicable in micro flow analysis systems, J. Micromech. Microeng. 9 (1999) 199.
[14] B. Baldyga, J.R. Bourne, B. Walker, Non-isothermal micromixing in turbulent liquids: theory and experiment, Can. J. Chem. Eng. 76 (1998) 641.